A Generalized Approach for Power Quality Disturbances Recognition Based on Kalman Filter

ABDELAZEEM A. ABDELSALAM[1], (Member, IEEE),
ALMOATAZ Y. ABDELAZIZ[2], (Senior Member, IEEE),
AND MOHAMED Z. KAMH[3], (Senior Member, IEEE)

[1]Department of Electrical Engineering, Faculty of Engineering, Suez Canal University, Ismailia 41522, Egypt
[2]Faculty of Engineering and Technology, Future University in Egypt, Cairo 11835, Egypt
[3]Department of Electrical Power and Machines Engineering, Faculty of Engineering, Ain Shams University, Cairo 11535, Egypt

Corresponding author: Abdelazeem A. Abdelsalam (aaabdelsalam@eng.suez.edu.eg)

This work did not involve human subject or animals in its research.

ABSTRACT This paper presents a new automatic detection and classification approach of power quality (PQ) problems using Kalman filter. Kalman filter is used as an estimator to calculate the fundamental frequency and harmonic components amplitudes of the voltage or current signals. Then the instantaneous total harmonic distortion (iTHD) and the energy are calculated. For each half cycle of the processed signal, five decision quantities are calculated based on iTHD and energy and these quantities are the three consecutive maximum values of iTHD, standard deviation and energy difference between distorted signal and its fundamental frequency component. Decision rules based on these decision quantities are applied to identify and classify the PQ events in this captured signal. The proposed approach is tested on single and combined PQ events that are generated using the MATLAB with the help of mathematical models that are conformity with standard IEEE-1159. The performance is assessed using more than 100 dataset of every PQ event and the results show that the accuracy is 100 and 98.8 for noiseless and high-level of noise, respectively. In addition, the proposed approach performance is validated through comparisons with other classification. Several practical PQ events are generated by lab experiments to validate the proposed approach. The simulation and experimental results show that the proposed approach is efficient and robust and can be implemented to design PQ monitoring device.

INDEX TERMS Feature extractions, harmonics, Kalman Filter, power quality.

I. INTRODUCTION

Power Quality (PQ) is becoming increasingly of a concern due to the increase of nonlinear loads and the proliferation of power-electronic interfaced distributed generation [1]. Poor PQ causes many issues such as mal-operation of protection devices, overheating of equipment leading to their failure, etc. Standard PQ problems such as sag, swell, interruption and flicker get exacerbated when harmonics are considered. [2]. Identification and classification of PQ problems in the voltage and current waveforms is the first step in mitigating effect of these problems [3]. PQ identification and classification are discussed in different works [4]–[6]. In the literature, the process of PQ identification and classification is two consecutive stages; viz.,(a) features extraction from the waveform and (b) problem classification.

Traditionally, Fourier transform (FT) and its modifications are the most common techniques used in PQ identification. Nevertheless, using FT loses the time information of the waveform [7]–[10]. This drawback is overcome by the wavelet transform (WT) [11]–[14]. Unlike FT, the WT decomposes the captured waveform in the time domain. WT performance depends on the selection of the mother wavelet and the number of decomposition layers [15]. The S-transform (ST) is also used to identify PQ events and it is an extension to wavelet transform [16]–[21]. ST decomposes the waveform in both time and frequency domains. However, ST is not practically common due to its hefty computational burden. Other signal processing algorithms such as Hilbert-Huang transform [22] and Gabor transform (GT) [23]

are used in PQ problems identification and classification but they suffer from large computational and running time.

One of the accurate signal-processing estimators is Kalman filter (KF). This technique applies a set of mathematical equations to calculate the states of a measured quantity. KF may result in inaccurate outputs if the state space model is incorrectly developed and/or if the choice of the KF parameters, e.g., process covariance (Q) and measurement covariance (R), is inaccurate [24]. In the literature, covariance values were chosen based on either optimal or heuristic based-methods.

Many algorithms are used to identify the optimal values of these noise covariance matrices. For example, in [25], two models for Q are provided for the steady state and transient estimation of power system harmonics. In [26], a reverse predication is used with Kalman filter to modify value of Q to enhance the filtering accuracy. In [27], the authors modified measurement covariance matrix R instead of process covariance Q. In [28], genetic algorithm and particle swarm optimization aided KF were proposed. In [29], the discrete wavelet transform is used to estimate the measurement covariance matrix. In [30], the extended Kalman filter is adapted using maximum likelihood. Albeit being the most accurate, optimal based-methods are known to increase the computation times and the complexity of implementation, and they cannot guarantee robustness with different noise levels [31].

Recently, the artificial intelligence techniques are used to classify PQ problems. These techniques include artificial neural network (ANN) [32], [33], probabilistic neural network (PNN) [34], support vector machine (SVM) [35], extreme learning machine (ELM) [36], K-nearest neighbor [37], decision tree (DT) [38], deep convolutional network [39] and long short-term memory networks [40]. These techniques have some shortages such as disability to classify complex PQ events and the need to be retrained in case of appearing a new PQ event [41].

A. RESEARCH GAP
All aforementioned works have many shortages such as:

- The use of two stages, feature extraction and classification to identify PQ problems and this increases the computational time.
- Some techniques cannot analysis big data and this decreases the accuracy.
- Some techniques cannot detect complicated problems such as sag with harmonics or swell with harmonics.
- Some techniques require a training period for each new PQ event.

For all these shortages, the need to an accurate, efficient, and automatic PQ problems detection technique is necessary.

B. WORK CONTRIBUTIONS
The main contributions of this work are:

- Proposing the Kalman filter to automatically detect (in real time) and heuristically classify PQ problems. The

proposed real-time detection approach does not need large memory because it stores only the previous state, very fast and well suited for online problems.
- Utilizing the fact that the voltage and current waveforms of modern power systems are sinusoidal waveforms that are distorted with harmonics that may be exceed or within the standard limits to models these waveforms by Kalman filter to estimate the amplitudes of the fundamental frequency and other harmonic orders as state variables with the help of the measured captured voltage or current waveforms
- Heuristic classification of PQ events (instead of using a computationally demanding algorithm as reported in the literature). From the estimated amplitudes, five decision quantities are calculated based on the instantaneous total harmonic distortion (iTHD) and energy. These quantities are the three consecutive maximum values of iTHD, standard deviation and energy difference between distorted signal and its fundamental frequency component.
- Implementing the proposed approach both in simulation and experimental setup to confirm its accuracy, simplicity, and robustness as a real-time application when subjected to wide spectrum of PQ events, Comparing the results of the proposed approach to those of other works is also conducted to confirm the validity of the proposed approach.
- Proving – through simulations and measurements – that the proposed approach is immune against impact of signal noise. The impact of errors that could occur during any stage starting from capturing the signal to the decision stage is studied to assess the performance of the proposed approach. These errors are represented as noise of different values of signal to noise ratio (SNR).

The rest of the paper is organized as follows. Section II presents the model of the generalized KF approach, together with the algorithm developed to implemented the new technique. Several PQ phenomena are simulated in Section III using the MATLAB platform, and the proposed generalized KF approach is used to detect and classify the PQ issues in the simulated waveforms. The new KF technique is used in an experimental setup to confirm the robustness of the tool and its practicality in Section IV. Conclusions are presented in Section V.

II. THE PROPOSED METHODOLOGY
At each sampling interval, the proposed generalized Kalman filter is used to estimate the amplitude of the fundamental frequency and harmonic components of the recorded waveform, and accordingly calculates the instantaneous total harmonic distortion of the signal. Moreover, for each half cycle, the model calculates some decision variables, viz., the energy of the harmonic contents, standard deviation and the maximum values of the calculated total harmonic distortion. This section introduces the principles of Kalman filter, its novel implementation as a generalized tool, and the details of the

decision variables that are used to classify the power quality disturbances.

A. PRINCIPLES OF KALMAN FILTER

Kalman algorithm is an estimator that is used to estimate the values of unknown variables with the help of observed measurements. To apply Kalman filter, initial steps should be prepared [29]:

- Modeling the state variable of the processes by preparing a relationship of state variables of the current step and the next step as follows:

$$x_{k+1} = \emptyset_k x_k + w_k \qquad (1)$$

- Iterative processing of the input signal that represents the noisy measurement, as follows:

$$Z_k = H_k x_k + v_k \qquad (2)$$

where: x_k and x_{k+1} are state variables at the current and next time steps k and $k + 1$, respectively, $\emptyset_k$ is a relationship matrix between x_k and x_{k+1} and is called the transition matrix, w_k is a row vector represents the state variables error, H_k is a matrix that represents the relationship between the noiseless measurements and the state variables and v_k is a row vector represents the measurements error. KF has two operation steps; prediction and correction. The prediction step updates the state variables and the associated error covariance using the following equations [29]:

$$\hat{x}_{k+1}^- = \emptyset_k \hat{x}_k^- \qquad (3)$$
$$P_{k+1}^- = \emptyset_k P_k \emptyset_k^T + Q_k \qquad (4)$$

where: $\hat{x}_{k+1}^-$ and $\hat{x}_k^-$ are prior estimated state variables at current, k, and next time step, $k + 1$, respectively, P_k and P_{k+1}^- are the a posterior and a prior estimated covariance of the process at current, k, and next time step, $k + 1$, respectively and Q_k is the covariance matrix of w_k.
The correction step updates Eq. (3) and Eq. (4) with the help of observable measurements, where Kalman gain K_k used in this step is defined in Eq. (5) [25]:

$$K_k = P_k^- H_k^T \left(H_k P_k^- H_k^T + R_k \right)^{-1} \qquad (5)$$

where: R_k is the covariance matrix of v_k.
With this estimated Kalman gain and the measured value Z_k, the state variables are updated using Eq. (6) [25]:

$$\hat{x}_k = \hat{x}_k^- + K_k \left(Z_k - H_k \hat{x}_k^- \right) \qquad (6)$$

where: $\hat{x}_k$ and $\hat{x}_k^-$ are posterior and prior estimated state variables at the time steps k.
The process covariance is updated by [25]:

$$P_k = (I - K_k H_k) P_k^- \qquad (7)$$

B. IMPLEMENTATION OF GENERALIZED KALMAN FILTER

In modern power systems, voltage and current waveforms are distorted sinusoidal waveforms due to harmonics associated with loads, non-linearities due to transformer saturation and inrush currents, as well as proliferation of power electronics. As such, voltage and current waveforms are expressed as sinusoidal functions with angular frequencies $i\omega$, where i is the harmonic order, and with sampling interval ΔT and time step k as follows:

$$Z_k = \sum_{i=1}^{n} A_i sin\left(i\omega k \Delta T + \theta_i \right) \qquad (8)$$

where A_i is the amplitude of the ith harmonic component.
The measured quantity at time instant $k + 1$ is expressed as:

$$Z_{k+1} = \sum_{i=1}^{n} A_i sin\left(i\omega \left(k + 1 \right) \Delta T + \theta_i \right) \qquad (9)$$

For each harmonic component, two state variables are modeled, with total number of state variables equals to 2n. The state variables are modeled as follows:
For fundamental harmonic order,

$$x_1 = A_1 \cos (\theta_1) \quad x_2 = A_1 \sin (\theta_1)$$

For 2nd order of harmonics,

$$x_3 = A_2 \cos (\theta_2) \quad x_4 = A_2 \sin (\theta_2)$$
$$\dots\dots\dots\dots \quad \dots\dots\dots\dots \qquad (10)$$

For nth order of harmonics,

$$x_{2n-1} = A_n \cos (\theta_n) \quad x_{2n} = A_n \sin (\theta_n)$$

The relationship between state variables at the current and next time steps is modeled by:

$$x_{k+1} = \begin{pmatrix} x_1 \\ x_2 \\ . \\ . \\ x_{2n-1} \\ x_{2n} \end{pmatrix}_{k+1} = \begin{bmatrix} 1 & 0 & \cdots & 0 & 0 \\ 0 & 1 & & 0 & 0 \\ & \vdots & \ddots & & \vdots \\ 0 & 0 & \cdots & 1 & 0 \\ 0 & 0 & & 0 & 1 \end{bmatrix} \times \begin{pmatrix} x_1 \\ x_2 \\ . \\ . \\ x_{2n-1} \\ x_{2n} \end{pmatrix}_{k} \qquad (11)$$

The measurement signal can be modeled as a relationship between state variables and matrix H as follows:

$$Z_k = H_k x_k = \begin{pmatrix} \sin (\omega k \Delta T) \\ \cos (\omega k \Delta T) \\ \vdots \\ \vdots \\ \sin (n\omega k \Delta T) \\ \cos (n\omega k \Delta T) \end{pmatrix}^T \begin{pmatrix} x_1 \\ x_2 \\ \vdots \\ \vdots \\ x_{2n-1} \\ x_{2n} \end{pmatrix}_{k} \qquad (12)$$
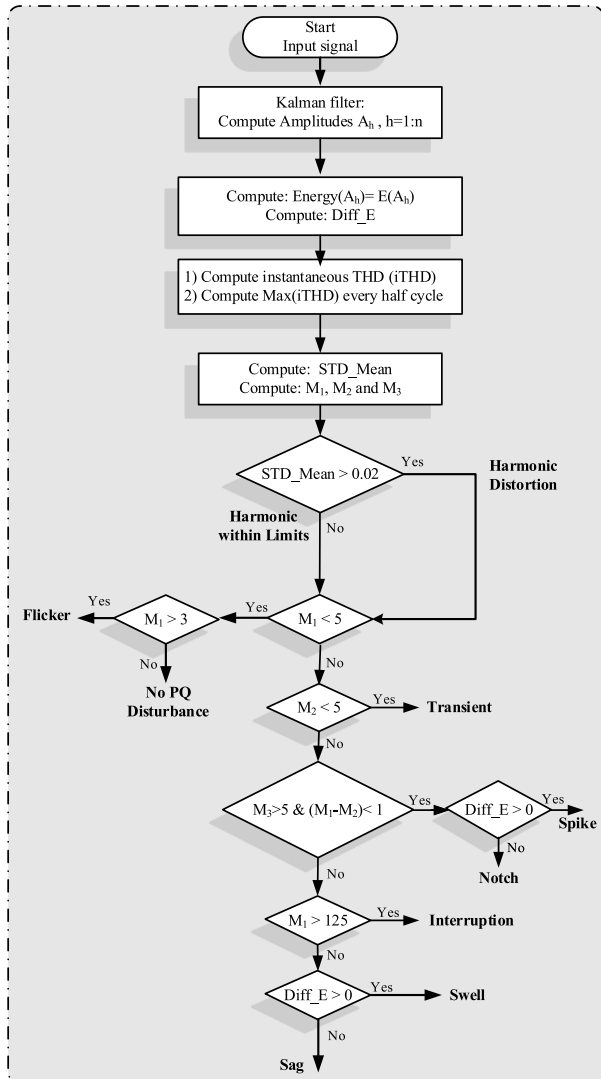
FIGURE 1. Flow chart of the proposed PQ classification approach technique.

The process noise covariance matrix Q_k, stated in Eq. (4), is chosen to be equal to the identity matrix in this model to provide fast tracking of variations in the system [25]. The measurement covariance matrix R_k, stated in Eq. (5), is chosen using an experience-based method.

At each time instant k, the state variables are estimated for each harmonic order to calculate the amplitudes and the instantaneous total harmonic distortion (*iTHD*).

The fundamental frequency amplitude is calculated by:

$$A_{1,k} = \sqrt{x_{1,k}^2 + x_{2,k}^2} \qquad (13)$$

The harmonic orders amplitude is calculated by:

$$A_{h,k} = \sqrt{x_{2h-1,k}^2 + x_{2h,k}^2} \quad i = 2, 3, \ldots, n \qquad (14)$$

The energy of this signal can be calculated by:

$$E_{distorted} = \sum_{i=1}^{n} A_{i,k}^2 \qquad (15)$$

The energy of harmonic distortions is the given by:

$$Diff\_E = E_{distorted} - E_{fundamental} \qquad (16)$$

The instantaneous total harmonic distortion (*iTHD*) is estimated by:

$$iTHD_k = \frac{\sqrt{A_{h,k}^2}}{A_{1,k}} \qquad (17)$$

For each half cycle of the measured signal, five quantities are calculated from the estimated *iTHD* as follows:

For each harmonic order, the mean value (M_e) is calculated by:

$$M_{e_i} = mean\,(A_i)\,i = 1, \quad 2, \ldots, n \qquad (18)$$

The standard deviation quantity is calculated by:

$$STD = STD \begin{pmatrix} M_{e2}/M_{e1} \\ M_{e3}/M_{e1} \\ \vdots \\ M_{e_{n-1}}/M_{e1} \\ M_{e_n}/M_{e1} \end{pmatrix} \qquad (19)$$

which represents the first quantity that is used in classifying the PQ problems. The second quantity is M_1 that represents first maximum value of instantaneous *iTHD*, the third quantity is M_2 that represents second maximum value of *iTHD*, the fourth quantity is M_3 that is the third maximum value of *iTHD* and the final value is the *Diff_E* for this half cycle. The classification of PQ problems is conducted using the values of the five decision variables, as shown in Fig. 1. The thresholds indicted in Fig. 1 are heuristically proposed.

III. SIMULATION RESULTS
A. GENERATION OF WAVEFORMS WITH PQ ISSUES
To illustrate the application of the proposed approach to detect and classify PQ problems, 16 different PQ events are generated using the equations depicted in Table 1 [20]. These events include the standard issues; sag, swell, interruption, flicker, transients, harmonics distortion, notch and spike, as well as combination of these issues MATLAB platform is used to generate the waveforms including the PQ issues. The effect of noise is taken into account by imposing noise signals to the main waveforms, with different signal to noise ratio (SNR) values of 20, 30 and 40 db. This noise represents the errors that could be occurred during the measurement, processing or classification stags. A sampling rate of 128 samples per cycle is used in the simulation environment.

TABLE 1. PQ modeling equations and their parameter values [20].

Disturbance class	Modeling Equations	Equations' Parameters
Normal	$h(t) = A\cos(\omega t)u(t)$	$A = 1\ pu, f = 50\ Hz, \omega = 2\pi f, u(t) = \begin{cases} 1, & t \geq 0 \\ 0, & t < 0 \end{cases}$
Sag	$h(t)=A\{1-k(u(t-t_1)-u(t-t_2))\}\cos(\omega t)$	$0.1<k<0.9,\ 0.5T \leq t_2-t_1 \leq 9T$
Swell	$h(t)=A\{1+k(u(t-t_1)-u(t-t_2))\}\cos(\omega t)$	$0.1<k<0.9,\ 0.5T \leq t_2-t_1 \leq 9T$
Interruption	$h(t)=A\{1-k(u(t-t_1)-u(t-t_2))\}\cos(\omega t)$	$0.9<k<1,\ 0.5T \leq t_2-t_1 \leq 9T$
Flicker	$h(t) = A[1+\alpha\cos(\beta\omega t)]\cos(\omega t)$	$0.1 \leq \alpha \leq 0.2,\ 0.1 \leq \beta \leq 0.4$
Transient	$h(t)=A\{\cos(\omega t)+k*exp[-(t-t_1)/\tau]\cos[\omega_n(t-t_1)]\}$	$0.1<k<0.8,\ 150 <1/\tau<1000$ $\omega_n = 2\pi f_n,\ 700\ Hz < f_n < 1600\ Hz$
Harmonics	$h(t)=A*\cos(\omega t)+\alpha_3\cos(3\omega t)+\alpha_5\cos(5\omega t)+\alpha_7\cos(7\omega t)$	$0.02<\alpha_3<0.1,\ 0.02<\alpha_5<0.1,\ 0.02<\alpha_7<0.1$
Notch	$h(t) = A*\cos(\omega t) - sgn(\cos(\omega t))$ $x\{\sum_{n=0}^{8}K[u(t-(t_1-0.02n))-u(t-(t_2-0.02n)]\}$	$0.1 \leq K \leq 0.4$
Spike	$h(t) = A*\cos(\omega t) + sgn(\cos(\omega t))$ $x\{\sum_{n=0}^{8}K[u(t-(t_1-0.02n))-u(t-(t_2-0.02n)]\}$	$0.1 \leq K \leq 0.4$
Sag with Harmonics	$h(t)=A\{1-k(u(t-t_1)-u(t-t_2))\}\cos(\omega t)$ $+ A\ p\ exp[-(t-t_3)/\tau]\ \cos[\omega_n(t-t_3)]$	$0.1<k<0.9,\ 0.5T \leq t_2-t_1 \leq 9T,\ t_1 \leq t_3 \leq t_2$ $0.1<p<0.8,\ 150 <1/\tau<1000$ $\omega_n = 2\pi f_n,\ 700\ Hz < f_n < 1600\ Hz$
Interruption with Harmonics	$h(t)=A\{1-k(u(t-t_1)-u(t-t_2))\}\cos(\omega t)$ $+ \alpha_3\cos(3\omega t)+\alpha_5\cos(5\omega t)+\alpha_7\cos(7\omega t)$	$0.9<k<1,\ 0.5T \leq t_2-t_1 \leq 9T,\ 0.02<\alpha_3<0.1,\ 0.02<\alpha_5<0.1,$ $0.02<\alpha_7<0.1$
Swell with Harmonics	$h(t)=A\{1+k(u(t-t_1)-u(t-t_2))\}\cos(\omega t) + \alpha_3\cos(3\omega t)+$ $\alpha_5\cos(5\omega t)+\alpha_7\cos(7\omega t)$	$0.1<k<0.9,\ 0.5T \leq t_2-t_1 \leq 9T,\ 0.02<\alpha_3<0.1,\ 0.02<\alpha_5<0.1,$ $0.02<\alpha_7<0.1$
Flicker with Harmonics	$h(t) = A[1+\alpha\cos(\beta\omega t)]\cos(\omega t) + \alpha_3\cos(3\omega t)+$ $\alpha_5\cos(5\omega t)+\alpha_7\cos(7\omega t)$	$0.1 \leq \alpha \leq 0.2,\ 0.1 \leq \beta \leq 0.4,\ 0.02<\alpha_3<0.1,\ 0.02<\alpha_5<0.1,$ $0.02<\alpha_7<0.1$
Transient with harmonics	$h(t)=A\{\cos(\omega t)+k*exp[-(t-t_1)/\tau]\cos[\omega_n(t-t_1)]\} +$ $\alpha_3\cos(3\omega t)+\alpha_5\cos(5\omega t)+\alpha_7\cos(7\omega t)$	$0.1<k<0.8,\ 150 <1/\tau<1000$ $\omega_n = 2\pi f_n,\ 700\ Hz < f_n < 1600\ Hz$ $0.02<\alpha_3<0.1,\ 0.02<\alpha_5<0.1,\ 0.02<\alpha_7<0.1$

TABLE 2. The extracted features of Case I.

Features	Sag and swell disturbances and normal event										
	Sag				Normal			Swell			
Magnitude	0.2	0.4	0.6	0.8	0.95	1	1.05	1.2	1.4	1.6	1.8
STD	0.0039	0.0028	0.0018	0.0008	0.0002	0.0000	0.0002	0.0008	0.0015	0.0022	0.0028
M_1	81.99	45.44	25.09	10.93	2.50	0.00	2.38	8.91	16.48	23.07	28.92
M_2	79.44	45.09	25.02	10.89	2.50	0.00	2.37	8.89	16.45	23.01	28.83
M_3	3.18	1.87	1.24	0.62	0.15	0.00	0.15	0.62	1.23	1.85	2.46
M_1-M_2	2.55	0.35	0.08	0.04	0.006	0.00	0.003	0.012	0.032	0.055	0.098
Diff_E	-0.1033	-0.0891	-0.0667	-0.0368	-0.0098	0.00	0.0102	0.0429	0.0913	0.1443	0.2015

B. RESULTS AND DISCUSSIONS

The generalized KF approach discussed in Section II is applied to analyze the waveforms descried in Section III-A. Results are presented in this section, including the impact of noise on the accuracy of the proposed technique.
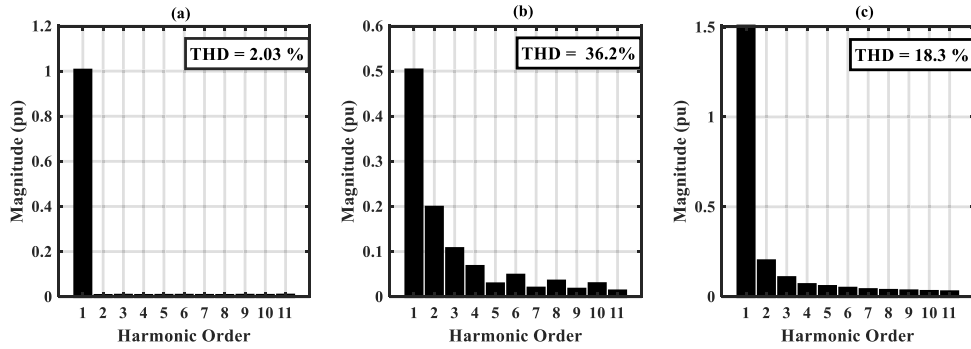
1) CASE I: NORMAL, SAG AND SWELL EVENTS

Normal sinusoidal waveforms are tested using the proposed approach and the required features are extracted and shown in Table 2. The STD feature value is less than 0.02 and this means that these normal signals do not contain harmonic distortions or the distortion is within limits. The frequency spectrum and the calculated iTHD are shown in Fig. 2(a). This figure shows that the magnitude of the fundamental component is 1 pu and the magnitude of the harmonic orders is very small and this is also depicted in Fig. 3 (b). Where the value of M_1 is less than 3 and this means there is no any PQ events in this processed signal. A sample example of normal signal is shown in Fig. 3.

Different case studies of the sag event are generated with different magnitudes; 0.2, 0.4, 0.6 and 0.8 pu. For these case studies, there is no harmonic contents because the STD value is less than 0.02 as shown in Table 2. The values of M1 and M2 are greater than 5 and M3 is less than 5 and this means that these events are interruption, sag or swell. Where the value of M1 is less than 125 then these events are sag or swell. To distinguish between sag and swell event, the value of last feature, Diff_E, should be checked.

Form Table 2, the values of these magnitudes, 0.2, 0.4, 0.6 and 0.8 are less than zero, negative values, and this means these case study events are sag. Fig. 4 shows an example of sag event with an amplitude of 1 pu. Fig. 4 (a) shows the waveform of the signal containing sag event. The amplitudes of fundamental frequency and other harmonic orders are shown in Fig. 4(b). The features M1 and M2 are shown in Fig. 4(d) and the value of M3 does not appear because it is very small in comparing with M1 and M2 values. The frequency spectrum at the starting instant of sag event is
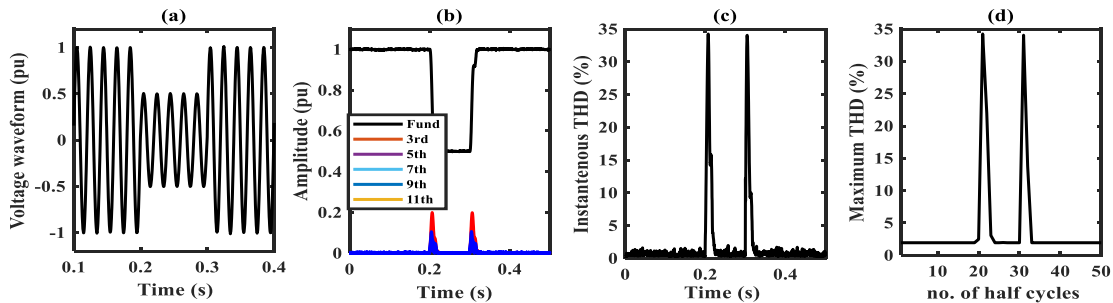
FIGURE 2. The frequency spectrum and iTHD at the starting of Case I events (a) Normal, (b) Sag, and (c) Swell events.
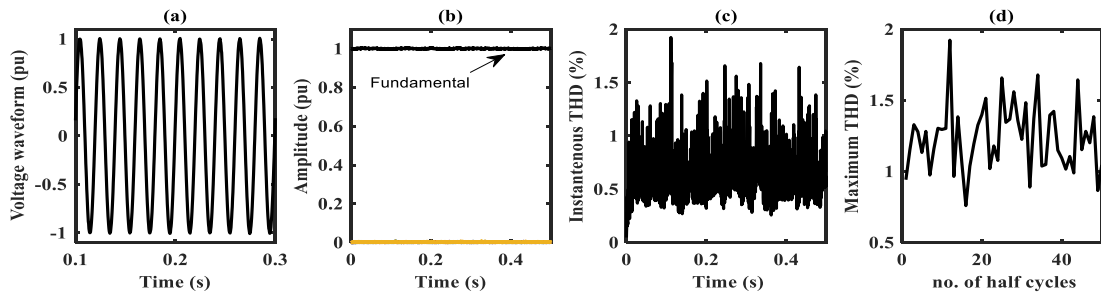
FIGURE 3. Case I: Normal event (a) waveform, (b) amplitudes, (c) iTHD and (d) Maximum values of iTHD.

FIGURE 4. Case I: Sag event (a) waveform, (b) amplitudes, (c) iTHD and (d) Maximum values of iTHD.

shown in Fig. 2(b). From this figure, it is clear that the magnitude of the fundamental frequency is 0.5 pu and the other harmonic orders have significant values and this causes that the iTHD is very high and equals 36.2 % at the starting of this event.

Fig. 5 shows an example of the swell event. Fig. 5 (d) shows that the values of M1 and M2 are high but less than 125 and this means that this event is sag or swell. From Table 2, it is found that the value of Diff_E is greater than zero and this means that this event is swell. In addition, the value of STD is less than 0.02 and this means that this signal does not contain harmonic distortions.

At the starting instant of the swell event, the calculated amplitudes of fundamental and harmonic orders using Eqs. (13) and (14) are shown in Fig. 2(c). The amplitude of the fundamental frequency is 1.5 pu and the other harmonic orders have significant values so the calculated iTHD is high and equals 18.3 %.

2) CASE II: INTERRUPTION EVENT

Table 3 shows different case studies of interruption events. The values of features M1 and M2 are greater than 5 and the value of M1 is greater than 125, indicating an interruption event has occurred. The values of STD feature are less than 0.02 and this means that these signals are pure sinusoidal waveforms. Fig. 6 shows the amplitudes of fundamental frequency and harmonic orders of the interruption waveform at the starting of this event. The figure shows that amplitudes of harmonic orders have high values where the amplitude of second and third orders are 0.38 and 0.2 pu, respectively, and this causes a high value of iTHD that reaches to 185%. Fig. 7 shows an example of interruption
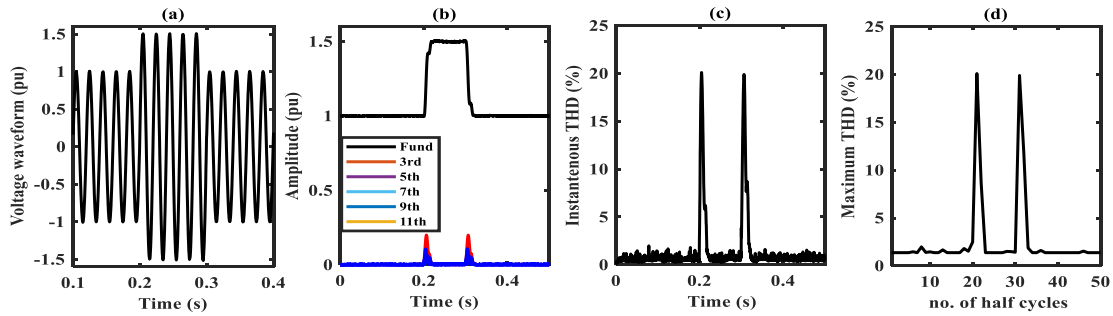
FIGURE 5. Case I: Swell event (a) waveform, (b) amplitudes, (c) iTHD and (d) Maximum values of iTHD.

TABLE 3. The extracted features of Case II.

Features	Interruption events									
Magnitude	0.01	0.02	0.03	0.04	0.05	0.06	0.07	0.08	0.09	0.1
STD	0.005	0.0049	0.0049	0.0048	0.0047	0.0047	0.0046	0.0046	0.0045	0.0044
M_1	347.50	293.30	251.44	215.79	185.10	159.96	146.16	139.02	132.01	125.22
M_2	202.0	174.15	152.12	141.72	135.68	129.98	124.61	119.53	115.18	111.03
M_3	8.44	7.30	6.65	11.01	8.67	7.12	6.02	5.80	5.60	5.50
M_1-M_2	145.5	123.15	99.32	74.07	49.42	29.97	21.55	19.48	16.83	14.19
Diff_E	-0.109	-0.1089	-0.1088	-0.1087	-0.1085	-0.1083	-0.1081	-0.1078	-0.1076	-0.1073
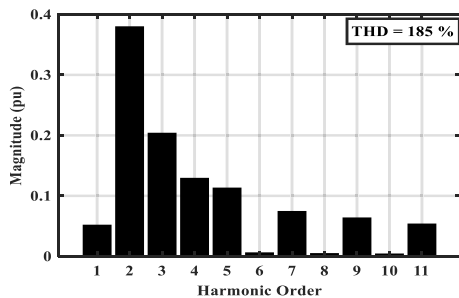
FIGURE 6. The frequency spectrum and iTHD at the starting of Case II: interruption event.

event where the values of M1 and M2 are 347.5 and 202, respectively.

3) CASE III: FLICKER EVENT

Fig. 8(a) shows a sinusoidal waveform with a flicker in the amplitude i.e., a change of the waveform amplitude but within the acceptable limits ($\pm$10%), which can be detected in the waveform envelope. The estimated amplitude of the waveform is shown in Fig. 8(b). The calculated maximum values of iTHD are shown in Fig. 8(d). From the flow chart of the proposed approach, the signal contains flicker if the value of M1 is between three and five. From Fig. 8(d), it is clear that the value of M1 is 3.5 and also the value of STD feature is less than 0.02 and this depicts that the waveform does not contain harmonic distortions. Fig. 9 shows the frequency spectrum and iTHD value for the flicker event. The amplitude of the fundamental frequency is 1 pu at the instant of calculation and the harmonic orders have very small amplitudes and this is shown in the value if iTHD that is 3.5 %.

4) CASE IV: TRANSIENT EVENT

The transient event is a sudden increase in the waveform magnitude for a very small duration of time. The calculated amplitudes of fundamental and harmonic orders using Kalman filter at the starting instant of this event are shown in Fig. 10. It is clear in this figure that the harmonic orders have high values and rises the iTHD to 156 %. The generated signal containing transient event is shown in Fig. 11(a). The value of M1 is shown in Fig. 11(d) and the value of M2 is very small and may not be existed. The STD value reveals that the signal is free of harmonic contents.

5) CASE V: HARMONIC DISTORTIONS EVENT

Different case studies of this event are generated by superimposing the sinusoidal waveform with harmonic distortions of THD; 10, 15, 20, 25, 30%. These signals are analyzed using the generalized KF methodology and the results are shown in Table 4. The values of STD are greater than 0.02 and this means that all tested signals contain harmonic. The value of M1 is less than three and this mean that there are no other PQ problems. Fig. 12 shows an example of a distorted signal by 20% THD.

6) CASE VI: NOTCH AND SPIKE EVENTS

The notch is a periodic decrease in the wave for a very small duration of time while the spike is a periodic increase. The frequency spectrum of the notch and spike event is almost the same as shown in Fig. 13. Fig. 14(a) shows the notch event waveform while the spike is shown in Fig. 15(a). Different cases of notch and spike event are tested and their extracted features are shown in Table 5. The features of notch and spike events are the same except the Diff_E values where Diff_E
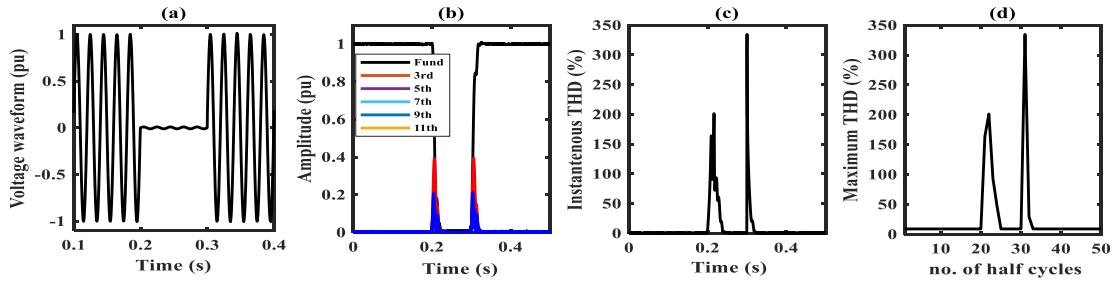
A. A. Abdelsalam *et al.*: Generalized Approach for PQ Disturbances Recognition

IEEE *Access*

FIGURE 7. Case II: Interruption event (a) waveform, (b) amplitudes, (c) iTHD and (d) Maximum values of iTHD.
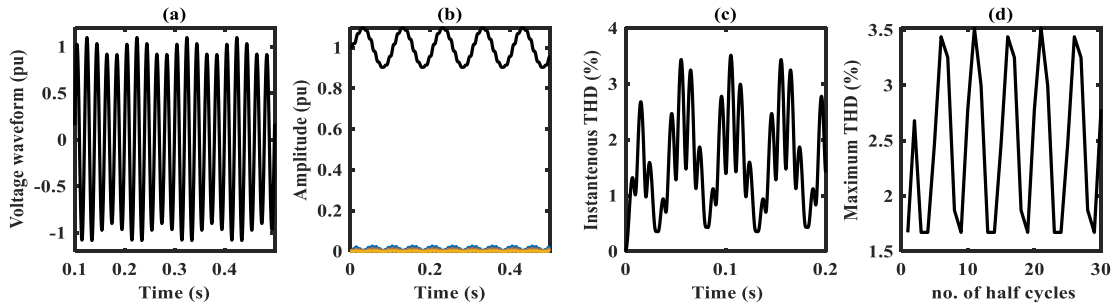

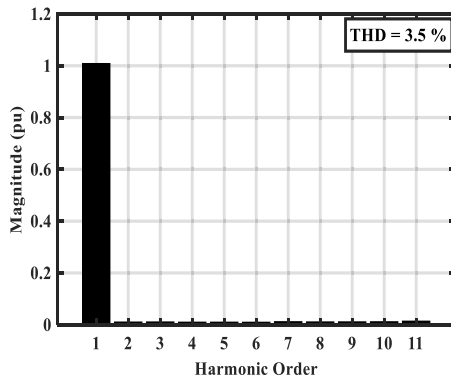**FIGURE 8.** Case III: Flicker event (a) waveform, (b) amplitudes, (c) iTHD and (d) Maximum values of iTHD.

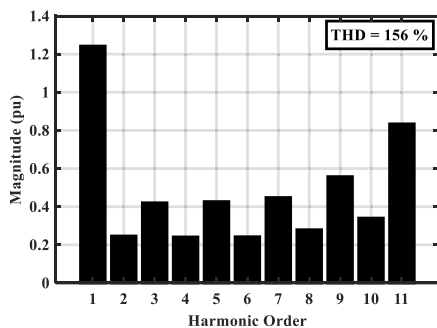**FIGURE 9.** The frequency spectrum and iTHD at the starting of Case III: flicker event.

FIGURE 10. The frequency spectrum and iTHD at the starting of Case IV: transient event.

values are negative for notch and positive for spikes, as shown in Table 5. Fig. 14 shows a sample example of the notch event and Fig. 15 depicts the waveform and features of spike event.

TABLE 4. The extracted features of Case V.

Features	Distorted Voltage				
THD	10	15	20	25	30
STD	0.676	0.73	0.79	0.88	0.96
M_1	2.66	2.493	2.375	2.488	2.611
M_2	2.514	2.446	2.354	2.444	2.520
M_3	2.382	2.378	2.347	2.379	2.383
M_1-M_2	0.146	0.047	0.021	0.044	0.091
Diff_E	1.32	1.66	1.97	2.65	3.37

TABLE 5. The extracted features of Case IV.

Features	Notch and Spike Disturbances			
Magnitude	Notch		Spike	
	0.1	0.2	0.1	0.2
STD	0.0002	0.0004	0.0002	0.0004
M_1	6.67	13.17	6.84	13.86
M_2	6.67	13.17	6.84	13.86
M_3	6.67	13.17	6.84	13.86
M_1-M_2	0.00	0.00	0.00	0.00
Diff_E	-0.002	-0.0044	0.0022	0.0044

7) CASE VII: SAG AND SWELL EVENTS WITH HARMONICS

In this case study, the sag or the swell events occur in a distorted signal. The results of processing different events of this case study using the proposed methodology are tabulated in Table 6. The STD values of all sag and swell events are greater than 0.02 indicating that the waveforms contain
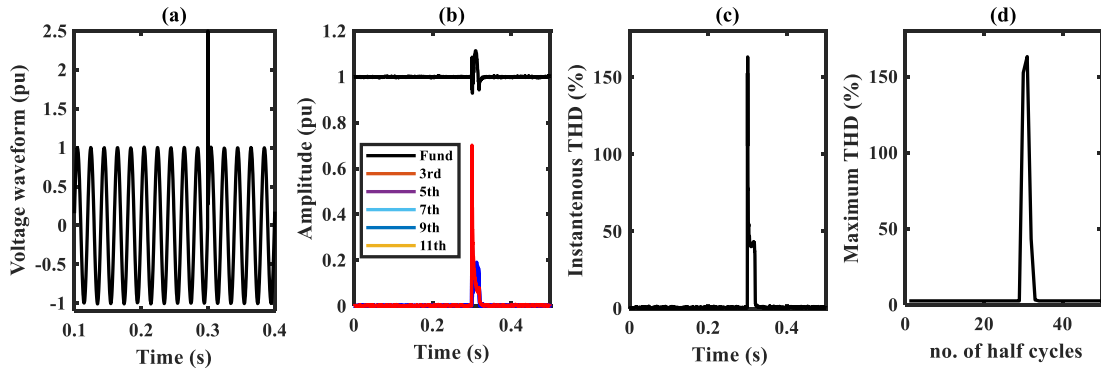
VOLUME 9, 2021

93621

FIGURE 11. Case IV: Transient event (a) waveform, (b) amplitudes, (c) iTHD and (d) Maximum values of iTHD.
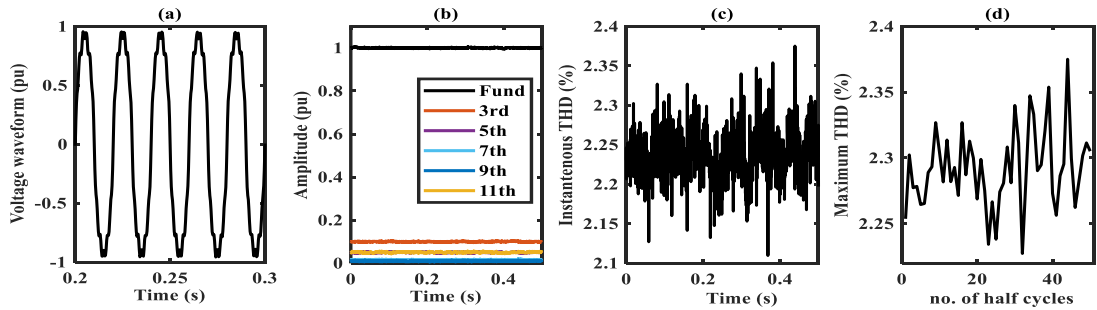

FIGURE 12. Case V: Harmonic distortions event (a) waveform, (b) amplitudes, (c) iTHD and (d) Maximum values of iTHD.
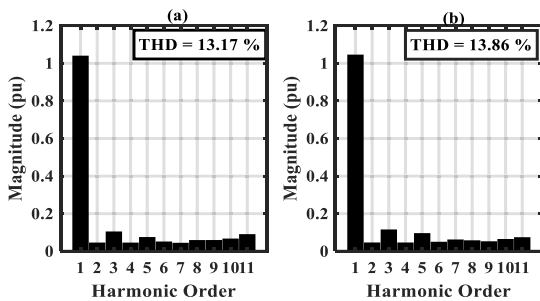

FIGURE 13. Case VI: The frequency spectrum and iTHD at the starting of (a) Notch and (b) Spike events.

TABLE 6. The extracted features of Cases VII and VIII.

Features	Sag			Swell		
Magnitude	0.2	0.5	0.8	1.2	1.5	1.8
STD	0.0039	0.0018	0.0008	0.0008	0.0022	0.0028
M_1	81.99	25.09	10.93	8.91	23.07	28.92
M_2	79.44	25.02	10.89	8.89	23.01	28.83
M_3	3.18	1.24	0.62	0.62	1.85	2.46
M_1-M_2	2.55	0.08	0.04	0.012	0.055	0.098
Diff_E	-0.103	-0.067	-0.037	0.043	0.144	0.202

harmonics. The values of features M1 and M2 are greater than 5 while the value of M3 is less than 5, i.e., sag or swell is detected. To distinguish between these two types of events, the value of Diff_E is used where positive Diff_E indicates a swell, and a negative Diff_E corresponds to a sag event. Fig. 16 shows an example of sag with harmonics event. The amplitudes of fundamental frequency and harmonics are shown in Fig. 16(b). The example of swell with harmonic event is shown in Fig. 17. The frequency spectrum of these two events at the starting instant are shown in Fig. 18. The amplitude of fundamental order of sag event is 0.5 pu while it is 1.4 pu for swell event. The iTHD values are close; 25.09 % and 21.4 % for sag, and swell sample example events, respectively. So iTHD values cannot be used to distinguish between these two events.

The other combined events, standard event with harmonics, are generated and tested using the proposed methodology. The results show that the STD values are greater than 0.02 and each event has its feature values that are used to identify its class using the decision variables shown in Fig. 1.

C. ERROR ANALYSIS

The impact of errors that could occur during the measurement, recording and processing stages of captured signals are studied. These errors are represented by a noise superimposed on the captured signals. More than 100 case studies are randomly generated for each PQ event, with different signal to noise ratios. The proposed approach is applied to identify the PQ issues in the case studies, and the results are shown in Table 7. The results show that with increasing the SNR,
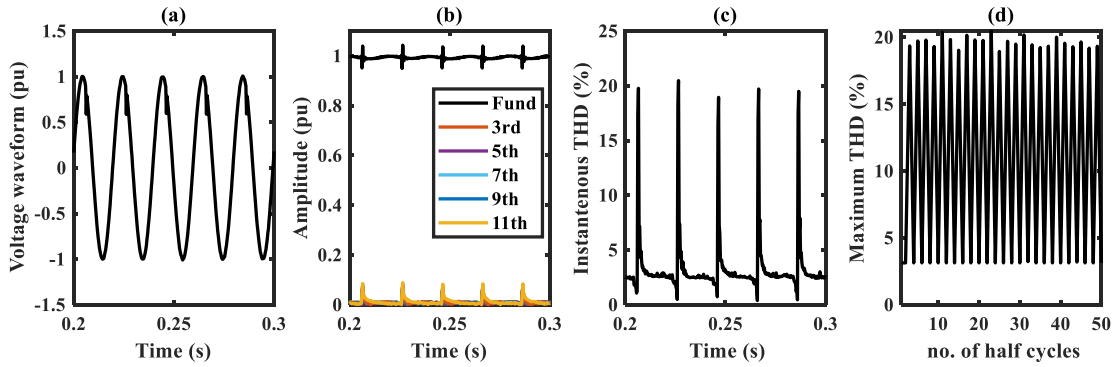
FIGURE 14. Case VI: Notch event (a) waveform, (b) amplitudes, (c) iTHD and (d) Maximum values of iTHD.
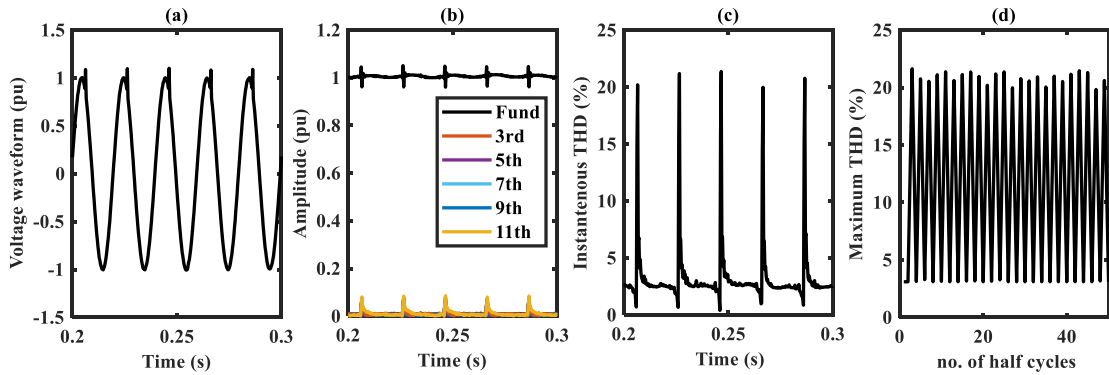

FIGURE 15. Case VI: Spike event (a) waveform, (b) amplitudes, (c) iTHD and (d) Maximum values of iTHD.
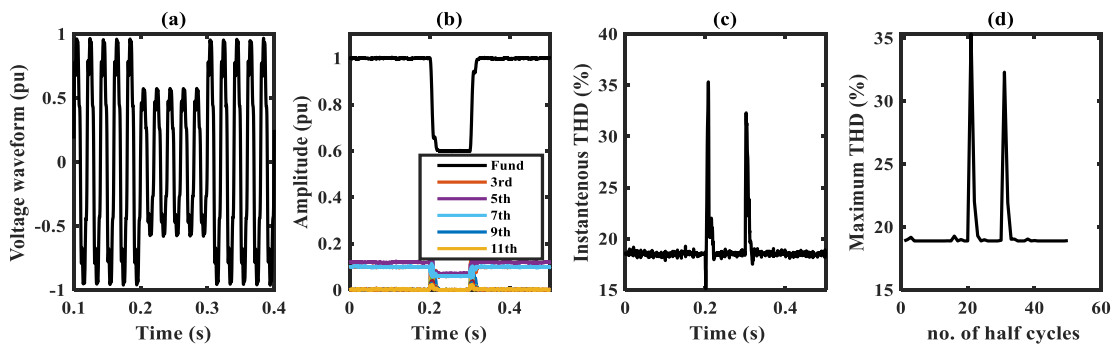

FIGURE 16. Case VII: Sag with harmonics event (a) waveform, (b) amplitudes, (c) iTHD and (d) Maximum values of iTHD.

the error decreases and thus, the estimated value closes to the actual value. The mean values of percentage error for the noiseless and the noisy conditions of 40 dB, 30 dB, and 20 dB are 0%, 0.07%, 0.3% and 1.2%, respectively, and the corresponding mean accuracies are 100%, 99.93%, 99.7%, and 98.8%, respectively. All case studies are running on MATLAB-2019b, Window 10, CPU; Intel core i7-2.7 GHz, 6 GB RAM.

The validation of the proposed approach is assessed by comparing its results with those of other works. The comparison results are tabulated in Table 8. The results show that the proposed approach has the ability to identify 16 classes of

PQ problems with high accuracy that equals to 100%, 99.93% and 99.7% for noiseless, 40 dB SNR and 30 dB SNR signals, respectively.

IV. EXPERIMENTAL RESULTS
To validate the proposed methodology in detecting and classifying the PQ events, an experimental model is established in the laboratory, as shown in Fig. 19. This model contains different types of loads to generate different types of power quality events. The loads comprise motors, linear and non-linear loads. Four potential transformers (PT) and four current transformers (CT) are used to step down the voltages
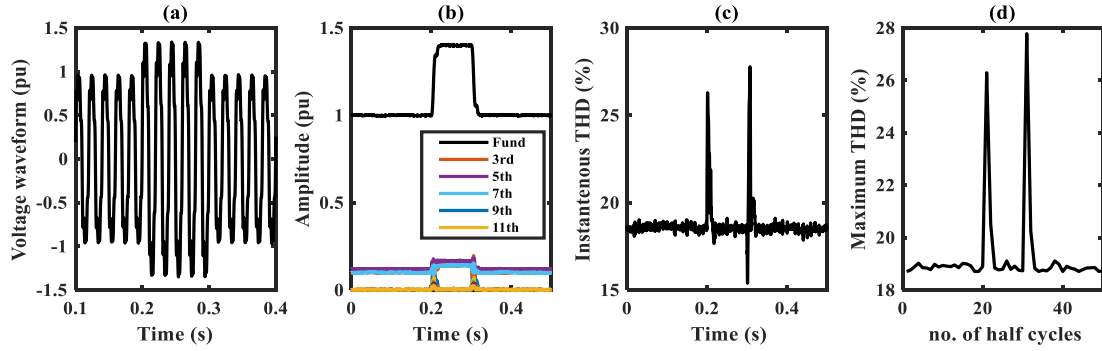
FIGURE 17. Case VII: Swell with harmonics event (a) waveform, (b) amplitudes, (c) iTHD and (d) Maximum values of iTHD.

TABLE 7. Simulation tests of PQ events with different SNR.

| PQ tested events	Error (%) and accuracy (%) at different noise levels						
	Noiseless	40 dB SNR		30 dB SNR		20 dB SNR	
	Accuracy (%)	Error (%)	Accuracy (%)	Error (%)	Accuracy (%)	Error (%)	Accuracy (%)
Normal	100	0.0	100	0.0	100	1.1	98.9
Sag	100	0.0	100	0.2	99.8	1.3	98.7
Swell	100	0.0	100	0.2	99.8	0.9	99.1
Interruption	100	0.1	99.9	0.4	99.6	1.2	98.8
Flicker	100	0.0	100	0.2	99.8	1.3	98.7
Transient	100	0.0	100	0.1	99.9	1.0	99
Harmonics	100	0.0	100	0.0	100	0.8	99.2
Notch	100	0.1	99.9	0.3	99.7	1.0	99
Spike	100	0.2	99.8	0.1	99.9	1.1	98.9
Sag with Harmonics	100	0.0	100	0.3	99.7	1.1	98.9
Swell with Harmonics	100	0.0	100	0.1	99.9	1.2	98.8
Interruption with Harmonics	100	0.2	99.8	0.5	99.5	1.3	98.7
Flicker with Harmonics	100	0.2	99.8	0.5	99.5	1.9	98.1
Transient with harmonics	100	0.1	99.9	0.6	99.4	1.2	98.8
Sag with Transients	100	0.1	99.9	0.7	99.3	1.4	98.6
Swell with Transients	100	0.1	99.9	0.6	99.4	1.5	98.5
Mean values	100	0.07	99.93	0.3	99.7	1.2	98.8
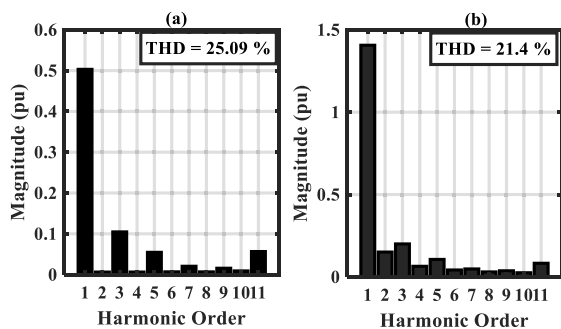
FIGURE 18. Case VII: The frequency spectrum and iTHD at the starting of (a) Sag with harmonics and (b) Swell with harmonics events.
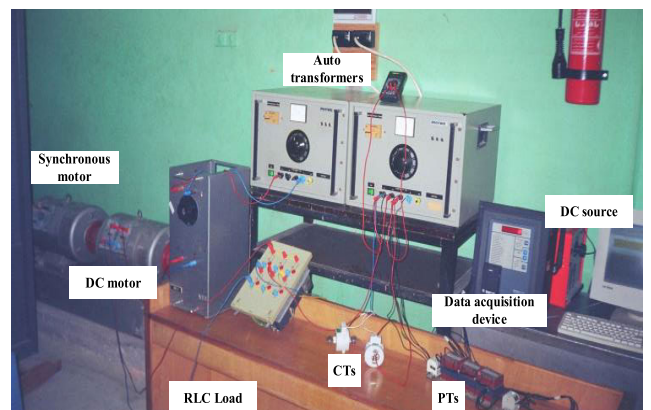

FIGURE 19. The experimental setup.

and currents to the data acquisition device to convert these captured waveforms from analog to digital form. The detailed parameters of this experimental model are provided in Table 9. The data acquisition device (DAS) is Circuit Monitor 2000 (CM2000) model. This DAS captures the voltage and current waveforms with 6.4 kHz (128 samples/cycle at 50 Hz) sampling frequency. Different case studies of PQ events are investigated and processed using the proposed

methodology. The results are explained in details in the following subsections.

A. CASE STUDY I

The experiment is run without nonlinear loads. The synchronous motor and linear RLC load are fed by the

TABLE 8. Comparison of classification accuracy with the existing methods.

Methods	Number of features	Number of tested PQ events	Mean accuracy (%)		
			NS	N40	N30
KF and FES [29]	2	7	-	98.71	97
FFT and ANNS [8]	-	8	-	93.95	95.65
WT and PSO-ELM [34]	6	10	97.6	-	-
WPT and SVM [14]	15	8	98.3	-	-
DWT and PNN [34]	9	16	99.87	98.6	95.2
ST and PNN [16]	4	11	97.4	-	-
ST and Dynamics [42]	5	12	-	99.27	97.91
LSTM [40]	6	14	-	97.45	95.25
MTW and DT [43]	4	13	99.9	-	-
Proposed Methodology	5	16	100	99.93	99.7

TABLE 9. Detailed parameters of the experimental model.

|	Parameter values
Sources	- AC voltage source: two 3- phase auto transformers of 0 – 400 V - DC variable voltage source: 0 - 220 V
Loads	- Synchronous Motor: 4.5 kW, 380V Delta, 7A and 220 V excitation - Nonlinear load represented by DC motor driven by 3-phase full wave bridge: 3.6 kW, 220 V DC, 20 A - Linear load: RL series load of 2.2 kW , 0.8 power factor
Current transformers	Four CT of turns ratio 50/5
Potential transformers	Four PT of turns ratio 380/110

FIGURE 20. The captured Voltage waveform of Case I.

autotransformers. For few milliseconds, the linear RLC load is disconnected. The voltage waveform, captured by DAS, is shown in Fig. 20.
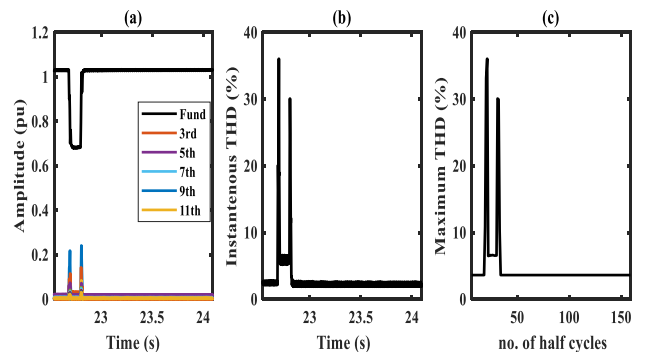
This waveform is passed to the proposed approach, where the extracted features are shown in Fig. 21 and Table 10. The values of the extracted features (STD, M1, M2, and Diff_E)
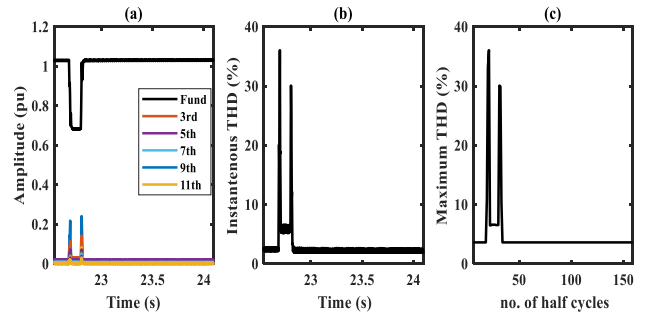
FIGURE 21. Case I (a) amplitudes, (b) iTHD and (c) Maximum values of iTHD.
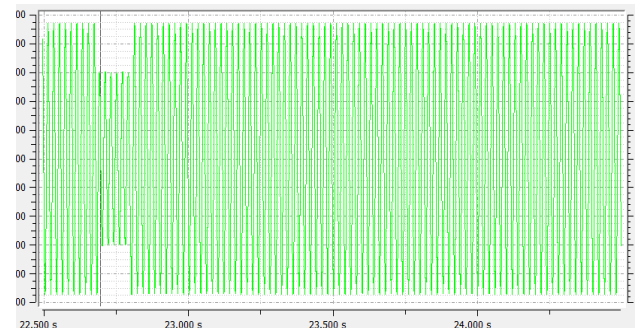
FIGURE 22. The captured waveform of Case I.

FIGURE 23. Case II (a) amplitudes, (b) iTHD and (c) Maximum values of iTHD.

are listed in Table 10. The values of the decision variables illustrate that this waveform does not contain harmonics and comprises a swell event.

B. CASE STUDY II

In this case study, the linear load is connected to the circuit for few milliseconds to generate a sag event. The voltage waveform, shown in Fig. 22, is captured by the (DAS) and transmitted to the PC to be processed by the proposed methodology. The extracted features are shown in Fig. 23 and Table 10. From Table 10, the STD is less than 0.02, corresponding to a waveform free of harmonics (no nonlinear loads were connected in this setup). The values of the other
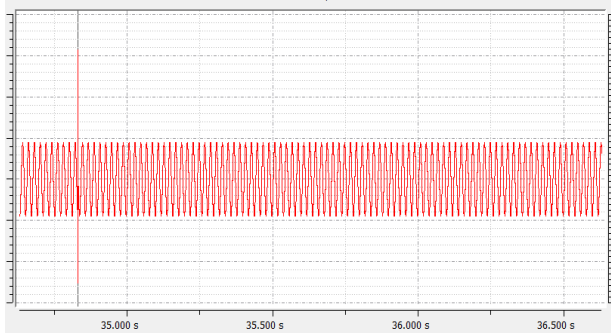
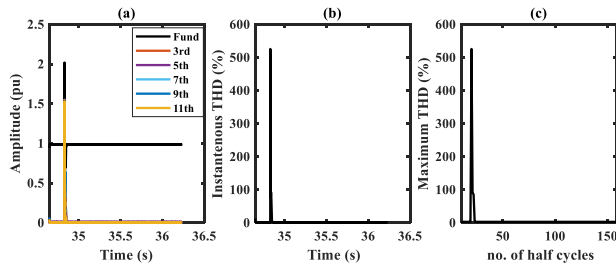**FIGURE 24.** The captured voltage waveform of Case III.

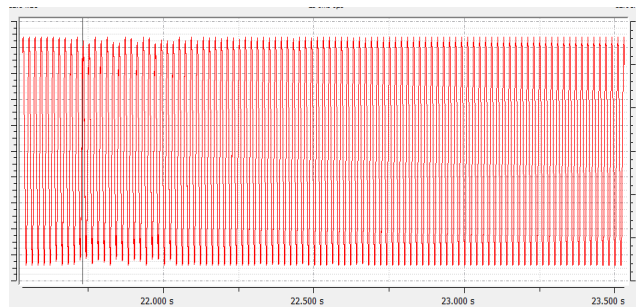**FIGURE 25.** Case III (a) amplitudes, (b) iTHD and (c) Maximum values of iTHD.

FIGURE 26. The captured waveform of Case IV.

FIGURE 27. Case IV (a) amplitudes, (b) iTHD and (c) Maximum values of iTHD.
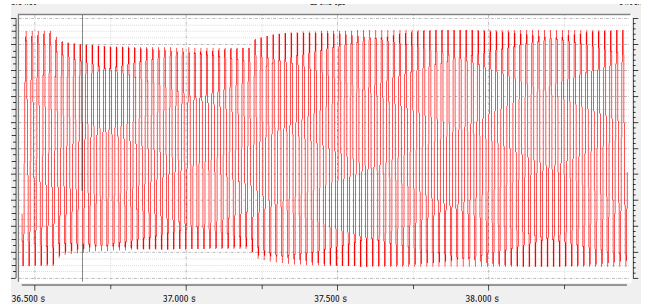
FIGURE 28. The captured voltage waveform of Case V.
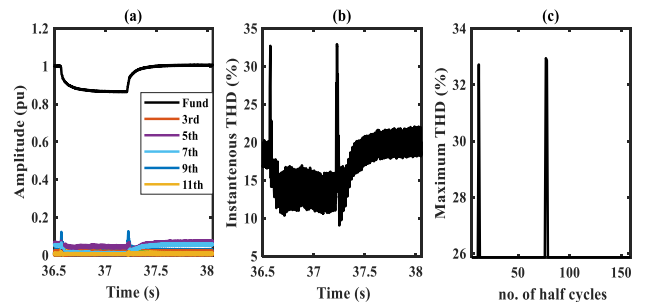
FIGURE 29. Case V (a) amplitudes, (b) iTHD and (c) Maximum values of iTHD.

TABLE 10. The extracted features of experimental case studies.

| Features | Experimental case studies | | | | |
	Case I	*Case II*	*Case II*	*Case IV*	*Case V*
STD	0.0055	0.0060	0.0037	0.038	0.041
M_1	12.7819	36.0613	525.576	2.865	32.95
M_2	12.0450	30.0929	0.104	2.338	32.72
M_3	0.05	6.64	0.00	2.111	0.00
M_1-M_2	0.7369	5.9684	421.667	0.527	0.23
Diff_E	5.6134	-5.4499	5.2693	5.2112	-5.0629
Class decision	Swell	Sag	Transient	Harmonics	Sag with harmonics

decision variables listed in Table 10 indicate that the captured waveform contains sag event.

C. CASE STUDY III

This case corresponds to a transient event imposed on a pure-sinusoidal waveform. To generate the transient event in this experiment, the linear load is switched off and on instantaneously. The captured voltage waveform is shown in Fig. 24. The extracted features are illustrated Fig. 25. In Fig. 25(c), M1 exceeds 125, indicating a transient event, while the corresponding STD in Table 10 indicates that the waveform does not contain harmonics.

D. CASE STUDY IV

In this case, all load types are connected to the circuit. The captured current waveform and extracted features are shown in Figs. 26 and 27, respectively. The Kalman filter computes the amplitudes of the fundamental frequency and harmonics
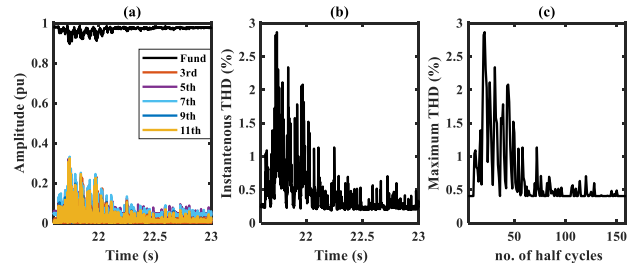
and these values are shown in Fig. 27(a). The calculated features for this case are shown in Table 10. The STD value is 0.038 and this means this waveform contain harmonics and the other features depicts that this current waveform does not comprises any other PQ events.

E. CASE STUDY V

In this case study, a complicated PQ event is generated by connecting all loads and disconnecting the linear load for few milliseconds. The captured current waveform is illustrated in Fig. 28. The proposed methodology processed this waveform and computes the amplitudes that are shown in Fig. 29(a). The values of M1, M2 and Diff_E in Table 10 confirm that this current waveform contains sag event. Considering the value of STD associated with this case, one can confirm that the waveform is polluted with harmonics.

V. CONCLUSION

In this paper, the power quality problem identification and classification are presented. A generalized approach based on Kalman Filters is developed and tested using simulation and experimental environments. The new approach is based on calculating five decision variables in real time. Based on the ranges of these variables, the algorithm decides whether the PQ issue is a sag, swell, transient, harmonics, etc. The thresholds proposed for these decision variables are heuristic. The simulation and experimental results have proven that these thresholds are accurate and dependable.

The simulation results for a wide range of cases are presented and analyzed. The results of the simulations – using the proposed approach – are compared against other reported techniques. The proposed approach proved its superiority to handle any kind of PQ events, even when noise is introduced to the waveforms. To confirm the practicality of the proposed KF method, an experimental setup was used to mimic different PQ events, with and without harmonics. The classification of the PQ events using the proposed approach were always correct and proved that it can be implemented to design PQ monitoring device.

REFERENCES

[1] A. F. Zobaa and S. H. E. A. Aleem, *Power Quality in Future Electrical Power Systems*. Edison, NJ, USA: IET, 2017.

[2] X. Liang, "Emerging power quality challenges due to integration of renewable energy sources," *IEEE Trans. Ind. Appl.*, vol. 53, no. 2, pp. 855–866, Mar. 2017.

[3] Y. Han, Y. Feng, P. Yang, L. Xu, Y. Xu, and F. Blaabjerg, "Cause, classification of voltage sag, and voltage sag emulators and applications: A comprehensive overview," *IEEE Access*, vol. 8, pp. 1922–1934, 2020.

[4] O. P. Mahela, A. G. Shaik, and N. Gupta, "A critical review of detection and classification of power quality events," *Renew. Sustain. Energy Rev.*, vol. 41, pp. 495–505, Jan. 2015.

[5] S. Khokhar, A. A. B. M. Zin, A. S. B. Mokhtar, and M. Pesaran, "A comprehensive overview on signal processing and artificial intelligence techniques applications in classification of power quality disturbances," *Renew. Sustain. Energy Rev.*, vol. 51, pp. 1650–1663, Nov. 2015.

[6] O. A. Alimi, K. Ouahada, and A. M. Abu-Mahfouz, "A review of machine learning approaches to power system security and stability," *IEEE Access*, vol. 8, pp. 113512–113531, 2020.

[7] T. X. Zhu, "Detection and characterization of oscillatory transients using matching pursuits with a damped sinusoidal dictionary," *IEEE Trans. Power Del.*, vol. 22, no. 2, pp. 1093–1099, Apr. 2007.

[8] F. A. S. Borges, R. A. S. Fernandes, I. N. Silva, and C. B. S. Silva, "Feature extraction and power quality disturbances classification using smart meters signals," *IEEE Trans. Ind. Informat.*, vol. 12, no. 3, pp. 824–833, Apr. 2016.

[9] J. Xu, Y. Zhang, Y. Li, and Y. Fan, "Comparative study of STFT and S transform on detecting voltage sag," *Power Syst. Protection Control*, vol. 42, no. 24, pp. 44–48, Dec. 2014.

[10] U. Singh and S. N. Singh, "Application of fractional Fourier transform for classification of power quality disturbances," *IET Sci., Meas. Technol.*, vol. 11, no. 1, pp. 67–76, Jan. 2017.

[11] D. De Yong, S. Bhowmik, and F. Magnago, "An effective power quality classifier using wavelet transform and support vector machines," *Expert Syst. Appl.*, vol. 42, nos. 15–16, pp. 6075–6081, Sep. 2015.

[12] H. Liu, F. Hussain, Y. Shen, S. Arif, A. Nazir, and M. Abubakar, "Complex power quality disturbances classification via curvelet transform and deep learning," *Electr. Power Syst. Res.*, vol. 163, pp. 1–9, Oct. 2018.

[13] K. Thirumala, M. S. Prasad, T. Jain, and A. C. Umarikar, "Tunable-Q wavelet transform and dual multiclass SVM for online automatic detection of power quality disturbances," *IEEE Trans. Smart Grid*, vol. 9, no. 4, pp. 3018–3028, Jul. 2018.

[14] M. Sahani, P. K. Dash, and D. Samal, "A real-time power quality events recognition using variational mode decomposition and online-sequential extreme learning machine," *Measurement*, vol. 157, Jun. 2020, Art. no. 107597.

[15] E. G. Ribeiro, T. M. Mendes, G. L. Dias, E. R. S. Faria, F. M. Viana, B. H. G. Barbosa, and D. D. Ferreira, "Real-time system for automatic detection and classification of single and multiple power quality disturbances," *Measurement*, vol. 128, pp. 276–283, Nov. 2018.

[16] S. Mishra, C. N. Bhende, and B. K. Panigrahi, "Detection and classification of power quality disturbances using S-transform and probabilistic neural network," *IEEE Trans. Power Del.*, vol. 23, no. 1, pp. 280–287, Jan. 2008.

[17] O. P. Mahela, A. G. Shaik, B. Khan, R. Mahla, and H. H. Alhelou, "Recognition of complex power quality disturbances using S-transform based ruled decision tree," *IEEE Access*, vol. 8, pp. 173530–173547, 2020.

[18] M. V. Reddy and R. Sodhi, "A modified S-transform and random forests-based power quality assessment framework," *IEEE Trans. Instrum. Meas.*, vol. 67, no. 1, pp. 78–89, Jan. 2018.

[19] N. Huang, D. Wang, L. Lin, G. Cai, G. Huang, J. Du, and J. Zheng, "Power quality disturbances classification using rotation forest and multi-resolution fast S-transform with data compression in time domain," *IET Gener., Transmiss. Distrib.*, vol. 13, no. 22, pp. 5091–5101, Nov. 2019.

[20] R. Kaushik, O. P. Mahela, P. K. Bhatt, B. Khan, S. Padmanaban, and F. Blaabjerg, "A hybrid algorithm for recognition of power quality disturbances," *IEEE Access*, vol. 8, pp. 229184–229200, 2020.

[21] T. Zhong, S. Zhang, G. Cai, Y. Li, B. Yang, and Y. Chen, "Power quality disturbance recognition based on multiresolution S-transform and decision tree," *IEEE Access*, vol. 7, pp. 8392–88380, 2019.

[22] R. Kumar, B. Singh, and D. T. Shahani, "Recognition of single-stage and multiple power quality events using Hilbert–Huang transform and probabilistic neural network," *Electr. Power Compon. Syst.*, vol. 43, no. 6, pp. 607–619, Apr. 2015.

[23] S. Naderian and A. Salemnia, "Method for classification of PQ events based on discrete Gabor transform with FIR window and T2FK-based SVM and its experimental verification," *IET Gener., Transmiss. Distrib.*, vol. 11, no. 1, pp. 133–141, Jan. 2017.

[24] J. Zhang, G. Welch, G. Bishop, and Z. Huang, "A two-stage Kalman filter approach for robust and real-time power system state estimation," *IEEE Trans. Sustain. Energy*, vol. 5, no. 2, pp. 629–636, Apr. 2014.

[25] K. K. C. Yu, N. R. Watson, and J. Arrillaga, "An adaptive Kalman filter for dynamic harmonic state estimation and harmonic injection tracking," *IEEE Trans. Power Del.*, vol. 20, no. 2, pp. 1577–1584, Apr. 2005.

[26] Z. Li and X. Wang, "Reverse prediction adaptive Kalman filtering algorithm for maneuvering target tracking," *J. Comput. Inf. Syst.*, vol. 6, no. 10, pp. 3257–3265, 2010.

[27] K.-R. Shih and S.-J. Huang, "Application of a robust algorithm for dynamic state estimation of a power system," *IEEE Trans. Power Syst.*, vol. 17, no. 1, pp. 141–147, Aug. 2002.

[28] R. K. Jatoth and G. A. Reddy, "A hybrid GA-adaptive particle swarm optimization based tuning of unscented Kalman filter for harmonic estimation," in *Proc. Int. Conf. Swarm, Evol., Memetic Comput. (SEMCCO)*, Chennai, India, Dec. 2010, pp. 380–388.

[29] A. A. Abdelsalam, A. A. Eldesouky, and A. A. Sallam, "Classification of power system disturbances using linear Kalman filter and fuzzy-expert system," *Int. J. Electr. Power Energy Syst.*, vol. 43, no. 1, pp. 688–695, Dec. 2012.

[30] Y. Xi, Z. Li, X. Zeng, and X. Tang, "Detection of voltage sag using an adaptive extended Kalman filter based on maximum likelihood," *J. Electr. Eng. Technol.*, vol. 12, no. 3, pp. 1016–1026, May 2017.

[31] Y. Xi, Z. Li, X. Zeng, X. Tang, Q. Liu, and H. Xiao, "Detection of power quality disturbances using an adaptive process noise covariance Kalman filter," *Digit. Signal Process.*, vol. 76, pp. 34–49, May 2018.

[32] R. Kumar, B. Singh, D. T. Shahani, A. Chandra, and K. Al-Haddad, "Recognition of power-quality disturbances using S-transform-based ANN classifier and rule-based decision tree," *IEEE Trans. Ind. Appl.*, vol. 51, no. 2, pp. 1249–1258, Mar. 2015.

[33] J. Wang, Z. Xu, and Y. Che, "Power quality disturbance classification based on compressed sensing and deep convolution neural networks," *IEEE Access*, vol. 7, pp. 78336–78346, 2019.

[34] S. Khokhar, A. A. M. Zin, A. P. Memon, and A. S. Mokhtar, "A new optimal feature selection algorithm for classification of power quality disturbances using discrete wavelet transform and probabilistic neural network," *Measurement*, vol. 95, pp. 246–259, Jan. 2017.

[35] P. Janik and T. Lobos, "Automated classification of power-quality disturbances using SVM and RBF networks," *IEEE Trans. Power Del.*, vol. 21, no. 3, pp. 1663–1669, Jul. 2006.

[36] R. Ahila, V. Sadasivam, and K. Manimala, "An integrated PSO for parameter determination and feature selection of ELM and its application in classification of power system disturbances," *Appl. Soft Comput.*, vol. 32, pp. 23–37, Jul. 2015.

[37] B. K. Panigrahi and V. R. Pandi, "Optimal feature selection for classification of power quality disturbances using wavelet packet-based fuzzy k-nearest neighbour algorithm," *IET Gener., Transmiss. Distrib.*, vol. 3, no. 3, pp. 296–306, Mar. 2009.

[38] T. Zhong, S. Zhang, G. Cai, and N. Huang, "Power-quality disturbance recognition based on time-frequency analysis and decision tree," *IET Gener., Transmiss. Distrib.*, vol. 12, no. 18, pp. 4153–4162, Oct. 2018.

[39] R. Gong and T. Ruan, "A new convolutional network structure for power quality disturbance identification and classification in micro-grids," *IEEE Access*, vol. 8, pp. 88801–88814, 2020.

[40] A. A. Abdelsalam, A. M. Hassanin, and H. M. Hasanien, "Categorisation of power quality problems using long short-term memory networks," *IET Gener., Transmiss. Distrib.*, vol. 15, no. 10, pp. 1626–1639, May 2021.

[41] G. S. Chawda, A. G. Shaik, M. Shaik, S. Padmanaban, J. B. Holm-Nielsen, O. P. Mahela, and P. Kaliannan, "Comprehensive review on detection and classification of power quality disturbances in utility grid with renewable energy penetration," *IEEE Access*, vol. 8, pp. 146807–146830, 2020.

[42] S. He, K. Li, and M. Zhang, "A real-time power quality disturbances classification using hybrid method based on S-transform and dynamics," *IEEE Trans. Instrum. Meas.*, vol. 62, no. 9, pp. 2465–2475, Sep. 2013.

[43] N. Huang, S. Zhang, G. Cai, and D. Xu, "Power quality disturbances recognition based on a multiresolution generalized S-transform and a PSO-improved decision tree," *Energies*, vol. 8, no. 1, pp. 549–572, Jan. 2015.

ABDELAZEEM A. ABDELSALAM (Member, IEEE) received the B.Sc., M.Sc., and Ph.D. degrees in electrical engineering from Suez Canal University, Egypt, in 2001, 2005, and 2011, respectively. He is currently an Associate Professor with Suez Canal University, Egypt. He was a Postdoctoral Fellow with the Institute of Technology (UOIT), University of Ontario, Canada. He has authored or coauthored more than 60-refereed journal and conference papers and three book chapters. His research interests include power quality, D-FACTS technology, switched filter compensators, micro-grid interface, and control and application of artificial intelligence techniques in power systems.

ALMOATAZ Y. ABDELAZIZ (Senior Member, IEEE) received the B.Sc. and M.Sc. degrees in electrical engineering from Ain Shams University, Cairo, Egypt, in 1985 and 1990, respectively, and the Ph.D. degree in electrical engineering according to the channel system from Ain Shams University, Egypt, and Brunel University, U.K., in 1996. He is a Professor at the Faculty of Engineering and Technology, Future University in Egypt, Cairo. He has been a Professor of electrical power engineering with Ain Shams University, since 2007. He has authored or coauthored more than 400 refereed journal articles and conference papers, 25 book chapters, and three edited books with Elsevier and Springer. His research interests include applications of artificial intelligence, evolutionary and heuristic optimization techniques to power system planning, operation, and control. He is a member of IET and the Egyptian Sub-Committees of IEC and CIGRE. He has been awarded many prizes for distinct researches and international publishing from Ain Shams University and Future University, Egypt. He is the Chairman of the IEEE Education Society chapter, Egypt. He is a Senior Editor of *Ain Shams Engineering Journal*, an Editor of *Electric Power Components and Systems Journal*, an editorial board member, an editor, an associate editor, and an editorial advisory board member for many international journals.

MOHAMED Z. KAMH (Senior Member, IEEE) received the B.Sc. (Hons.) and M.Sc. degrees in electrical power and machines engineering from Ain Shams University, Cairo, Egypt, in 2003 and 2007, respectively, and the Ph.D. degree in electrical engineering from the University of Toronto, Toronto, ON, Canada, in 2011. He is currently an Assistant Professor with the Department of Electrical Power and Machines Engineering, Ain Shams University. His research interests include power system planning and operation, power electronics, distributed and renewable energy resources, smart grids, and application of artificial intelligence in the aforementioned fields. He serves as the Technical Adviser for the Ministry of Electricity and Renewable Energy for Transmission Network planning and operation. He is a Registered Professional Engineer in Egypt, and the Provinces of Alberta and Ontario, Canada, where he served for more than a decade as a utility leader in the fields of transmission system planning, operation, and engineering.

• • •